Working Paper

Climate Simulations with an Improved 2-D Zonal Climate Model

Andrey V. Ganopolski
and
Jaroslav Krabec

WP-94-22
April, 1994

IIASA International Institute for Applied Systems Analysis □ A-2361 Laxenburg □ Austria
Telephone: +43 2236 715210 □ Telex: 079 137 iiasa a □ Telefax: +43 2236 71313

Climate Simulations with an Improved 2-D Zonal Climate Model

Andrey V. Ganopolski and Jaroslav Krabec

WP-94-22

April 1994

International Institute for Applied Systems Analysis ☐ A-2361 Laxenburg Austria

Telephone: +43 2236 715210 ☐ Telex: 079137 iiasa a ☐ Telefax: +43 2236 71313

FOREWORD

The climate research component of the Forestry and Climate Change Project has had as one of the objectives to develop a series of simplified climate models which can be part of integrated models for analyses of climate change. This Working Paper describes climate simulations with an improved 2-D zonal climate model.

TABLE OF CONTENTS

ABSTRACT

An improved version of the 2-D Zonal Climate Model in comparison with that published in the preceeding paper (Jonas et al., 1993) is presented. The modifications introduced lead to a closer agreement of the global energy distribution with current estimates and to a more complex behaviour of the coupled model, namely to the occurence of internal oscillations in the climate system on a decadal time scale.

The results give additional support to the idea that simplified climate models can be successfully used as a climatic part of integrated models of climate change.

1. Introduction

In a previous paper (Jonas et al., 1993, referred to as *WP1*), a two-dimensional Zonal Climate Model (2-D ZCM), which couples atmospheric and oceanic modules, was presented as one of the climate models available or under development at IIASA for purposes of integrated modelling of climate change impacts. In this paper a detailed description of the model and its results, the latter for the simulation of present climate, the equilibrium response due to a doubling of atmospheric CO_2 and several time-dependent experiments, was given illustrating that the model can indeed be used for the investigation of various climate impacts.

In the paper we present an improved version of the 2-D ZCM. Several modifications were introduced in the descriptions of both atmosphere and ocean. The modifications of the atmosphere lead to a better distribution of energy in the climate system and to an increased of climate sensitivity in comparison to the previous model version. Some of the modifications are the introduction of a coefficient for horizontal diffusion that is dependent on the temperature gradient; inclusion of a lapse rate feedback; and the replacement of the heat capacity of dry air by that of moist air. The main improvement of the oceanic part is the inclusion of salinity as an independent variable. It is well known that the salinity has an important impact on the density field and, as a result, on baroclinic circulation and vertical mixing. Recent experiments with oceanic General Circulation Models (GCMs) suggest that the salinity can help to explain the complex behaviour of the climate system, i.e., instabilities, oscillations and existence of different stationary states. The inclusion of salinity permits to make the parameterization of vertical overturning in the ocean more physically

sound and to decrease the number of prescribed model parameters.

The structure of the Working Paper is as follows: in Part 2 atmospheric and oceanic parts of the model are described. Part 3 presents model results - simulation of current climate, internal variability, climate sensitivity and a time-dependent response. We conclude the paper with Part 4.

2. Description of the 2-D ZCM

2.1 Atmospheric component

The structure of the atmospheric component of the 2-D ZCM is described in detail in the previous paper (*WP1*). Therefore, we only recapitulate briefly the main features of the model and rather describe the changes introduced into the model in the following.

The atmospheric model is based on energy balance principles. It distinguishes eighteen latitude belts with a horizontal resolution of 10 degrees latitudinally and eight basic model layers in the atmosphere vertically. The surface corresponds to a surface pressure of 1000 hPa. The model describes mean annual conditions. It is steered by the concentrations of a number of greenhouse gases such as H_2O, CO_2, CH_4, N_2O, CFC-11, CFC-12 and O_3.

2.1.1 Energy balance for the atmosphere

For the evaluation of atmospheric temperatures in the eigth basic model layers the following

equation is used:

$$\frac{\partial T}{\partial t} = A + Q_S + Q_I + Q_L \quad , \tag{1}$$

where T is the atmospheric temperature in the individual layers, t is time, Q_S, Q_I and Q_L are heating rates due to solar radiation, infrared radiation and latent heat release, and A represents the net effect of the redistribution of thermal energy by dynamical mechanisms.

Radiative fluxes result from the radiative transfer scheme of the MacKay and Khalil's (1991) 1-D Radiative Convective Model. The scheme requires a more detailed vertical structure consisting of eighteen vertical layers; the resulting radiative fluxes are evaluated only at the top and bottom of each basic layers, however. Cloudiness is treated in the scheme as a single effective cloud layer, height and optical thickness of which are tuning parameters that vary latitudinally. For the computation of latent heat release, total precipitation is computed at first as the difference between surface evaporation and vertically integrated divergence of water vapour. The latent heat released in individual atmospheric layers is then found by means of a vertical distribution function. The last term, redistribution of thermal energy by dynamical mechanisms, is based on a diffusion approach. For vertical transport the vertical turbulent coefficient is set at the top of the boundary layer (top of the first model layer) and it decreases exponentially with height. For horizontal transport the diffusion coefficient was set a constant value in the previous paper (*WP1*). In this paper, the horizontal diffusion coefficient is computed based on a temperature gradient:

$$D = K \, |\Delta T| \quad , \tag{2}$$

where ΔT is temperature difference between successive latitudinal belts,

$K = 0.25*10^6$ m^2 s^{-1} K^{-1} (Sellers, 1973).

Another change, which influences Eq. 1, is that the specific heat of dry air is replaced by the specific heat of moist air throughout the entire model. In this paper the approximate relationship:

$$c_p = c_{pd} (1 + 0.9\ q) \quad , \tag{3}$$

is used, where c_{pd} is the specific heat of dry air (1004.64 J kg^{-1} K^{-1}) and q the water vapour mixing ratio.

Because of the dependence of specific heat on height, two additional changes were introduced:

a) The dry convective adjustment scheme, which is used at the end of each integration step, has to conserve $\int c_p\ T\ dp$. Changes in the water vapour profile are not taken into account in the conservation requirement because of the basic model assumption that the relative humidity remains constant with time. Therefore, water vapour content changes only with changing temperature and thus has to be recalculated when the temperature profile is modified by the convective adjustment.

b) Because of the finer vertical resolution required by the radiative transfer scheme (eighteen layers in comparison with the eight basic model layers), a vertical interpolation from the basic to the finer vertical structure is necessary. This vertical interpolation also conserves $\int c_p\ T\ dp$.

2.1.2 Energy balance for the surface

At the surface, three surface types are distinguished with respect to surface temperature computations: land, sea ice and open ocean. While the equation for the oceanic temperatures will be given in Part 2.2, the energy balance equations applied to land and sea ice read:

$$C_L \frac{\partial T_L}{\partial t} = S_L - I_L - H_L - LE_L \quad ,$$
$$C_I \frac{\partial T_I}{\partial t} = S_I - I_I - H_I - LE_I + q_I \quad , \tag{4}$$

where S is the shortwave radiative flux absorbed by the surface, I the net surface flux of thermal radiation (positive upward), H and LE are the sensible and latent heat fluxes, respectively. Indices L and I refer to land and sea ice. C stands for the effective heat capacity of the surface, q_I refers to the heat flux through sea ice. The surface radiative fluxes are computed in the radiative transfer scheme.

With respect to surface albedo, the land is further subdivided into free land and land covered with snow. While albedos of free land and open ocean are prescribed for individual latitude belts and held constant with time; albedo of land covered by snow and albedo of sea ice are parameterized in terms of fractional extent of snow cover on land and fractional extent of sea ice, respectively. The fraction of the land covered with snow is a function of the surface air temperature above land, which is parameterized following Peng et al. (1987). The fraction of ocean covered by sea ice is a function of mixed layer temperature. Surface sensible and latent heat fluxes are computed by means of bulk formulations, utilizing the differences between surface and surface air temperature and water vapour mixing ratio, respectively.

As mentioned already, a convective adjustment scheme is used at the end of each time step. In *WP1*, a prescribed critical lapse rate of $\gamma = 6.5$ K km^{-1} was used. In this study, the critical lapse rate is not constant any more but it is allowed to change with surface air temperature (Mochov, 1983):

$$\gamma = a_0 + a_1 T_S \quad , \tag{5}$$

where T_S is the latitudinally averaged surface air temperature, $a_1 = 0.04$ km^{-1} and values of a_0 for individual latitude belts are given in the following table:

latitudinal belt	a_0 [K km^{-1}]
90 - 80 N	-5.584
80 - 70 N	-5.584
70 - 60 N	-5.372
60 - 50 N	-5.286
50 - 40 N	-5.552
40 - 30 N	-5.534
30 - 20 N	-5.912
20 - 10 N	-5.714
10 N - Eq.	-5.656

Tab. 1

For the Southern hemisphere, the same list of values is used correspondingly (e.g., -5.583 K km^{-1} for 80-90 S).

The parameterization leads to a good approximation of the averaged tropospheric lapse rate in the model, i.e., the decrease of the lapse rate from the equator (about 6.5 K km^{-1}) towards the poles (about 4.2 K km^{-1}) is well described and also the local minima in subtropical

regions are reflected by the model.

2.2 Oceanic component

In the present version of the zonal advective-diffusive ocean model, the world ocean is represented by one ocean basin. There are a few significant differences in comparison with the version described in *WP1*. These are 1.inclusion of salinity as an independent variable; 2. an improved parameterization of the baroclinic circulation; 3. implementation of the equation of state as given by UNESCO (1981); and 4. spatialy dependent coefficients of diffusion. The parameterization of sea ice is the same as described in *WP1*.

2.2.1 Temperature and salinity equations

The equation for the zonally averaged temperature and salinity can be written in a general form for the oceanic mixed layer (ML)

$$h_1 \frac{\partial X_1}{\partial t} = -\frac{1}{Rl}\left[\frac{\partial}{\partial \varphi}(\Psi_1 X_1) - \frac{\partial \Psi_1}{\partial \varphi} X^*\right] + \frac{h_1}{R^2 l}\frac{\partial}{\partial \varphi}(A_\varphi l \frac{\partial X_1}{\partial \varphi}) + q_0^X - q_1^X, \qquad (6)$$

and for the deep ocean layers

$$\frac{\partial X}{\partial t} = -\frac{1}{Rl}\left[\frac{\partial}{\partial \varphi}(\frac{\partial \Psi}{\partial z} X) - \frac{\partial}{\partial z}(\frac{\partial \Psi}{\partial \varphi} X)\right] + \frac{1}{R^2 l}\frac{\partial}{\partial \varphi}(A_\varphi l \frac{\partial X}{\partial \varphi}) + \frac{\partial}{\partial z}(A_z \frac{\partial X}{\partial z}), \qquad (7)$$

where X is the potential temperature (T) or salinity (S), X_1 is the ML temperature or salinity, X^* the same, but for the bottom of ML, $l = l(\varphi)$ is the latitudinal oceanic extension, R the earth radius, and $h_1 = 50\ m$ the mixed layer depth. A_φ and A_z the coefficients of horizontal (meridional) and vertical diffusion, which are now dependent on φ and z, Ψ is the vertical overturning stream function (VOSF), and Ψ_1 the VOSF at the bottom of the ML. The vertical temperature and salinity fluxes at the ocean surface and at the bottom of the ML are determined by

$$q_0^T = \left[(1-f_I)(S_O - I_O - H_O - LE_O) + f_I q_I\right](c\rho)^{-1},$$
$$q_0^S = S^*(E_O - P_O - R_O), \tag{8}$$

and

$$q_1^X = -A_z \left.\frac{\partial X}{\partial z}\right|_{z=h_1+\varepsilon}, \tag{9}$$

where S_O is the absorbed solar radiation, I_O the outgoing longwave radiation flux at the ocean surface, H_O and LE_O are the sensible and latent heat fluxes at the ocean surface, q_1 is the heat flux through sea ice, P_O the precipitation over ocean, R_O the zonally averaged runoff, c_p the specific heat capacity of sea water, ρ the density of sea water, and $S^* = 35$ ppt is the so-called "reper salinity".

2.2.2 Equation of state

In the present version of the model, the equation of state is used in the form given by

UNESCO (1981)

$$\rho(T,S,p) = \frac{\rho^*(T_s,S,0)}{1 - \dfrac{p}{p_k(T_s,S,p)}}, \tag{10}$$

where $p = \rho g z$ is the pressure,

$$\begin{aligned} \rho^*(T_s,S,0) &= a_0 + a_1 T_s + a_2 T_s^2 + a_3 S + a_4 T_s S + a_5 S^{3/2} + a_6 T_s S^{3/3} + a_7 S^3, \\ p_k(T,S,p) &= b_0 + b_1 T_s + b_2 T_s S + b_3 p + b_4 T_s p + b_5 T_s S, \end{aligned} \tag{11}$$

T_s is so-called "*in situ*" (measured) temperature, which is related with potential temperature T by

$$T_s = \frac{T + c_1 p + c_2 p^2}{1 - c_3 p}, \tag{12}$$

and a_i, b_i, c_i are empirical coefficients.

The potential density, which determines the vertical stability of the water column and, thus the situations when convective adjustment procedure is applied, is given by

$$\rho_p = \rho^*(T,S,0). \tag{13}$$

2.2.3 Model dynamics

The total VOSF is reproduced in the model as a sum of winddriven and baroclinic components:

$$\Psi = \Psi_w + \Psi_b, \tag{14}$$

The winddriven component Ψ_w is determined using Ekman mass transport in the ML

$$\Psi_w = - \frac{\tau_x \, l}{\rho_0 \, f} \psi_0(z) \ , \tag{15}$$

where τ_λ is the zonally averaged zonal component of wind stress, derived from Han and Lee (1983), f the Coriolis parameter, H_b = 4000 m the ocean bottom depth and

$$\psi_0(z) = \begin{cases} \dfrac{z}{h_1} \ , & z \le h_1 \\ \dfrac{H_b - z}{H_b - h_1} \ , & z > h_1 . \end{cases} \tag{16}$$

For determination of baroclinic component Ψ_b, an approach similar to that described in Wright and Stocker (1991) is used. The zonally averaged meridional baroclinic component of current velocity $V_b = \frac{1}{l} \frac{\partial \Psi_b}{\partial z}$ is supposed to be proportional to the meridional gradient of pressure anomaly (deviation from vertically averaged) p':

$$\frac{\partial \Psi_b}{\partial z} = k(\varphi) \frac{\partial p'}{\partial \varphi} . \tag{17}$$

Taking into account that

$$p(z) = p(0) + \rho g z, \qquad and \qquad \int_0^{H_b} p'(z) dz = 0 . \tag{18}$$

one can obtain from Eqs. 17 and 18 the following expression for the baroclinic component of VOSF:

$$\Psi_b(z) = k(\varphi)\int_0^z \left[-\frac{g}{H_b}\int_0^{H_b}(H_b - z'')\frac{\partial\rho}{\partial\varphi}dz'' + g\int_0^{z'}\frac{\partial\rho}{\partial\varphi}dz'' \right] dz' . \tag{19}$$

It follows directly from Eqs. 11 and 19 that

$$\Psi(0) = \Psi(H_b) = 0 .$$

The function $k(\varphi)$ was chosen in the form of Wright and Stocker (1991)

$$k(\varphi) = \varepsilon \cos(\varphi) . \tag{20}$$

where ε is a tuning parameter.

2.2.4 Coefficients of diffusion

To parameterize the effects of meridional heat (salt) transport in the ocean by mechanisms other than vertical overturning, the coefficient of horizontal diffusion was enhanced in the upper baroclinic layer ($z \leq 1$ km) and in latitudinal belts, where intensive horizontal circulation gyres exist. The coefficient of horizontal diffusion was determined by

$$A_\varphi = A_\varphi^{\max} f_1(\varphi) f_2(z) , \tag{21}$$

where

$$f_1(\varphi) = \begin{cases} C_1, & |\varphi| \geq \varphi^* \\ C_1 + C_2 \sin^2 \dfrac{2\varphi}{\varphi^*}, & |\varphi| < \varphi^* \end{cases} \qquad (22)$$

$$f_2(z) = C_3 + C_4 \exp(-\frac{z}{1000}),$$

and $A_\varphi^{max}=4 \cdot 10^3$ m^2/s, $C_1=0.3$, $C_2=0.7$, $C_3=C_4=0.5$, $\varphi^*= 60°$. Thus the coefficient of horizontal diffusion has the maximum in subtropical region, where horizontal circulation and mesoscale eddies are the most intensive. A_φ decreases with depth on typical vertical thermocline scale (1 km).

There is an increasing number of empirical evidences that coefficient of vertical diffusion in the ocean interior (beneath the upper ocean layer) increases with depth and that its value in the main thermocline is much smaller than it is commonly used in oceanic models (order of 0.1 cm^2/s). Following Cuminis et al. (1990), we used a dependence of A_z on a vertical density stability characteristics, the Brunt-Väisälä frequency N:

$$A_z = a_0 N^{-1}, \qquad where \qquad N = \left[-\frac{g}{\rho} \frac{\partial \rho_p}{\partial z} \right]^{1/2} \qquad (23)$$

and $a_0 = 10^{-3}$ cm^2/s^2. The following restrictions for A_z in case of a stable density stratification were also used:

$$0.1 < A_z < 10 cm^2/s. \qquad (24)$$

In case of an unstable stratification, the application of the convective adjustment procedure practically means an infinitely large coefficient of vertical diffusion.

2.2.5 Salinity flux

There are a few options to determine freshwater flux to the ocean. The most natural one is to use freshwater flux computed by the atmospheric module as the difference between precipitation, evaporation, and runoff in each latitudinal belt. Another possibility is to use zonally averaged freshwater flux based on observation. But as numerios GCMs results show (Manabe and Stouffer, 1988; Weaver and Sarachik, 1991a), the ocean circulation is very sensitive to freshwater flux, and the use of realistic freshwater fluxes can produce unrealistic salinity and circulation fields. For this reason, another approach is commonly utilized in oceanic modelling, namely, freshshwater flux is determined by Newtonial relaxation term

$$q_0^s = \frac{h_1}{\tau_{rel}}(S_{obs} - S_1), \tag{25}$$

where S_{obs} is the observed surface salinity and τ_{rel} is the relaxation time. This approach allows to reproduce the salinity distribution reasonably well, but it may not be justified for investigations of the climate sensitivity or transient climate changes. Indeed, changes of salinity field can be very important for global climate change, while the use of freshwater flux in form given by Eq. 25 does not allow for significant changes of the salinity field. That is why the following procedure (the so-called "mixing surface boundary conditions", Weaver and Sarachik, 1991a) is usually used. On the first stage of an experiment, when equilibrium state of the climate system is computed, the freshwater flux is described by the Eq. 25. When the system reached the equilibrium, the salinity flux is averaged in time during a few decades to eliminate short-periodic variations. During the next stage, when the behaviour of the entire climate sysem is investigated, this salt flux is used as prescribed

(time-independent). This procedure was used in the present study. The relaxation time was chosen τ_{rel} = 90 day. To describe correctly deep water characteristics, S_{obs} was determined as observed salinity below mixed layer rather than surface one. The meanannual zonally averaged data for depth 100m from Levitus (1982) were used.

3. Model results

In the preceding paper (*WP1*), quite a detailed description of the behaviour of the previous model version was given, for 1. the simulation of present climate, 2. the equilibrium response to a doubling of atmospheric CO_2, and 3. several scenarios with increasing greenhouse gas concentrations. In this paper, we concentrate only on the most important differences in comparison with *WP1* and on ne features of the model like, e.g., the internal variability on a decadal time scale.

3.1 Simulation of current climate

Figure 1, (taken from Schneider, 1989), shows the energy balance of the earth in comparison to the solar input; the solar "constant" (1368.3 W m^{-2} used in this study) divided by four represents 100%. The numbers in the brackets correspond to the current estimation, while the underlined values result from the model. This comparison shows that the model overestimates the current estimate of the planetary albedo by approximately 2% (the reflected solar radiation of the model is 32.1% compared to 30% given in Schneider, 1989). It is worth mentioning that the model was not tuned with respect to planetary albedo, the same set of main parameters as in *WP1* (first of all, height of the effective cloud layer and cloud

optical thickness in each latitude belt) was used. Consequently, the outgoing thermal radiation at the top of the atmosphere (TOA) is underestimated correspondingly. The total energy imbalance at the TOA (the net radiative flux) is only of the order of 0.01 W m^{-2}. The fluxes balance also at the surface, the sum of both absorbed solar flux and downward thermal radiation has to be equal to the sum of the thermal radiation emitted by the surface and the sensible and latent heat fluxes. There are some differences in the individual fluxes between the current estimation and the model result, the biggest of which is for the thermal outgoing surface radiation (104% according to the current estimation vs. 116% in the model). However, the overall picture indicates quite a good agreement of the model with the real energy balance of the earth.

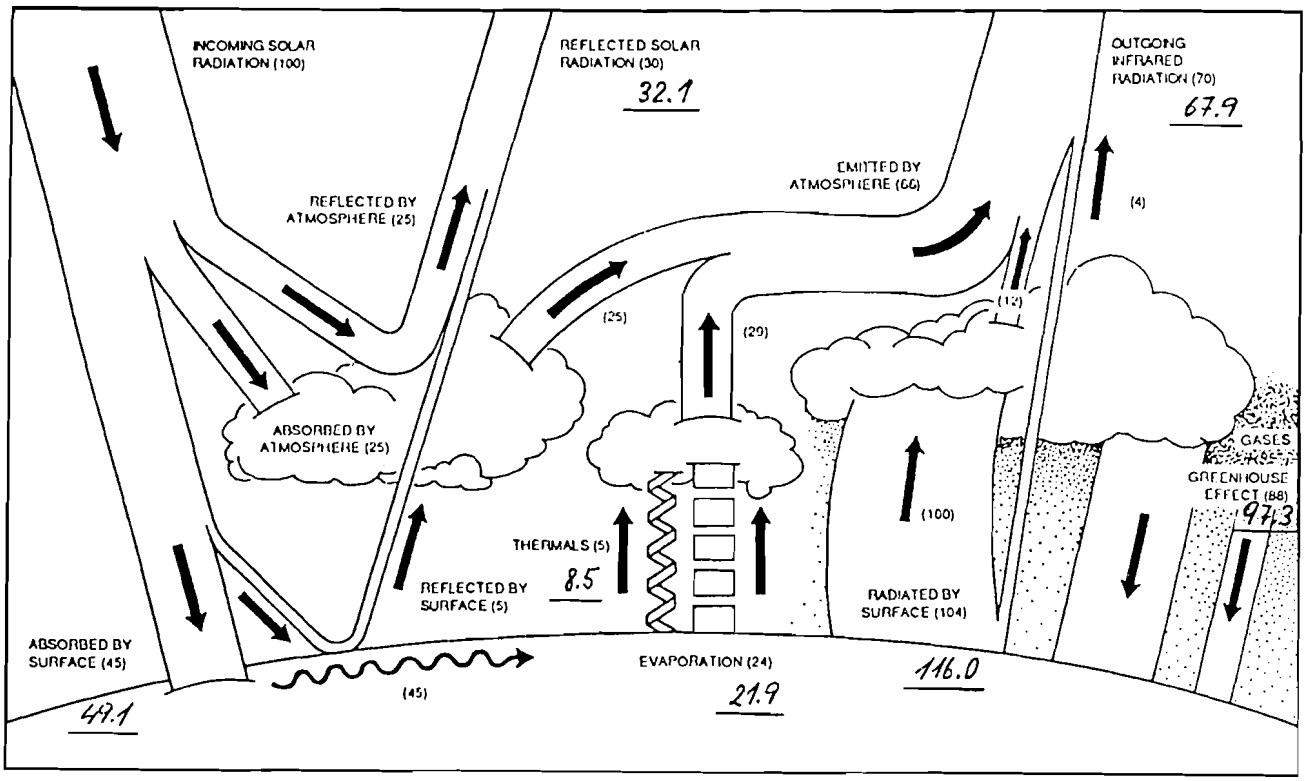

Fig. 1. Energy distribution for current climate (Schneider, 1989). Included are model results (underlined values).

Figure 2 gives more information about the planetary albedo, showing the albedo at the TOA by latitude. The albedo reproduced by the model is in a good agreement with estimates given by Smith and Smith (1987) and Ellis and Vonder Haar (1976) except in low latitudes, where the model gives higher values. This leads to the overestimation of the albedo of the whole planet mentioned above.

Another significant change in the behaviour of the model was caused by letting the horizontal diffusion coefficient be dependent on the latitudinal temperature gradient, instead of being constant. In Figure 3 the meridional heat transport in the atmosphere (1 PtW = 10^{15} W) computed by the model is compared with estimates given by Carissimo et al. (1985) and with the results of the previous model version (using a constant diffusion coefficient). The current model gives a significantly better agreement with the Carissimo's data as far as the maximum values in the middle latitudes are concerned. On the other hand, the agreement is worse in the low latitudes where the heat transport is overestimated.

The salinity field, which is a new prognostic variable of the oceanic model, is shown in Figure 4. Realistic distribution of salinity in the surface layer is ensured by the form chosen for the salinity flux, while the salinity distribution in the ocean interior reflects the model's ability to reproduce the propagaiton of active tracers. The two regions of deep water formation are at 60-70 N and 70-80 S. In agreement with observed data, northern deep water has a higher salinity than the near Antarctic deep water and it is also warmer. One of the most important features of the real salinity field, the tongue of intermediate Antarctic water masses of lower salinity, which propagates northward at 1 km depth, is correctly reproduced by the model. At the same time, the model freshwater flux, (cf. Figure 5), is not in good

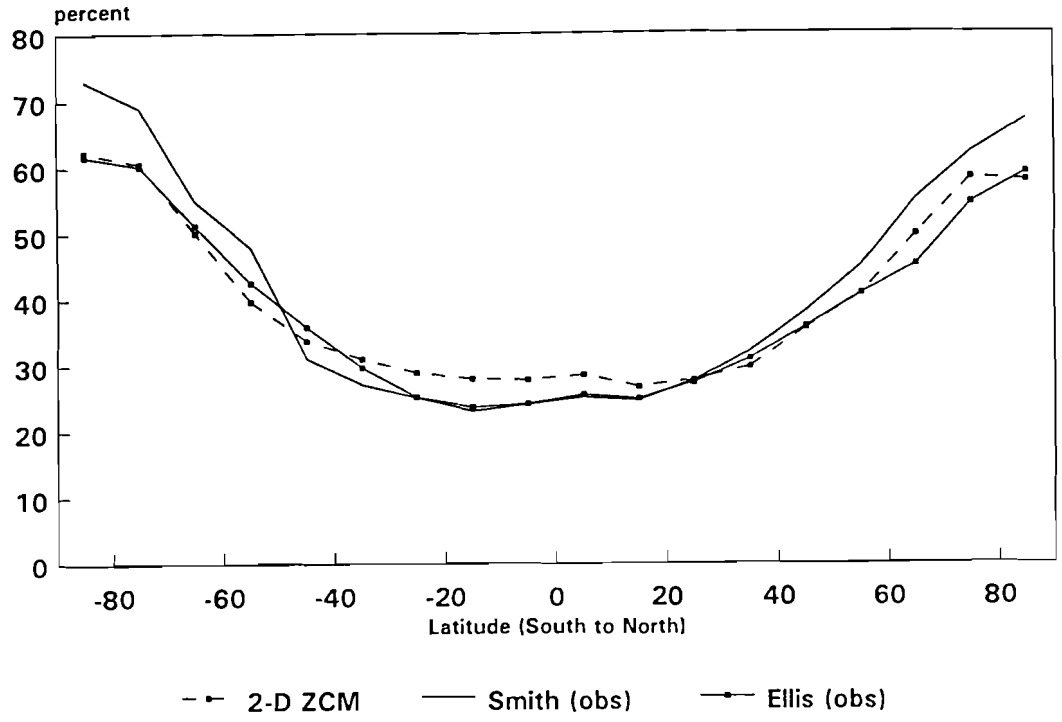

Fig. 2. Latitudinal distribution of the albedo at the TOA.

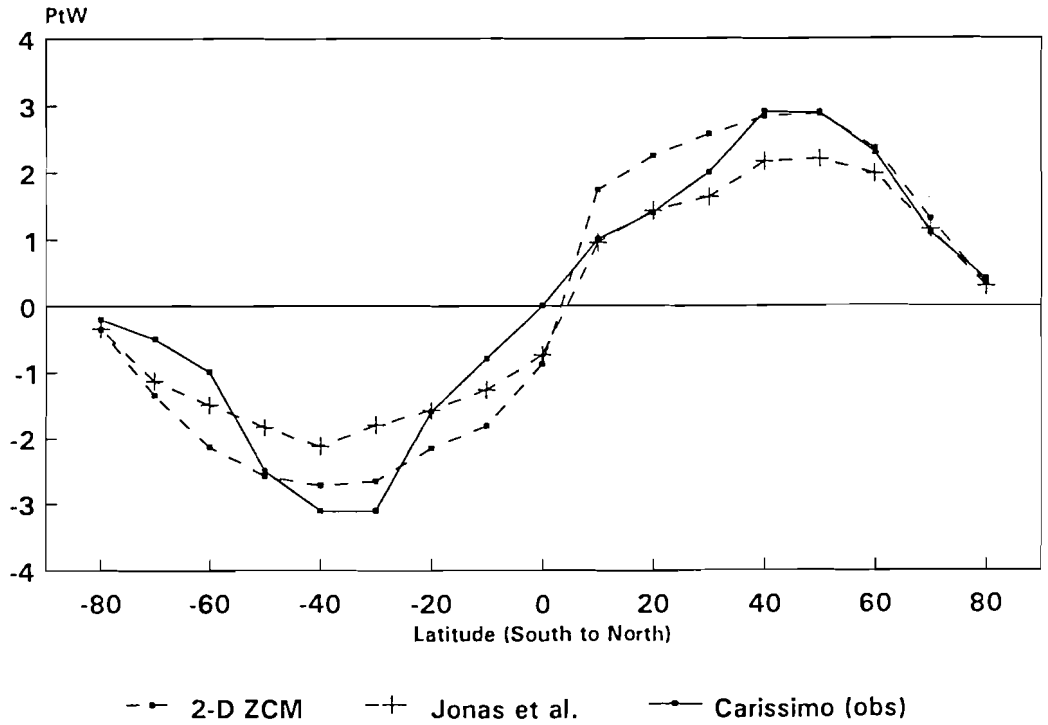

Fig. 3. Meridional heat transport in the atmosphere (1 PtW = 10^{15} W).

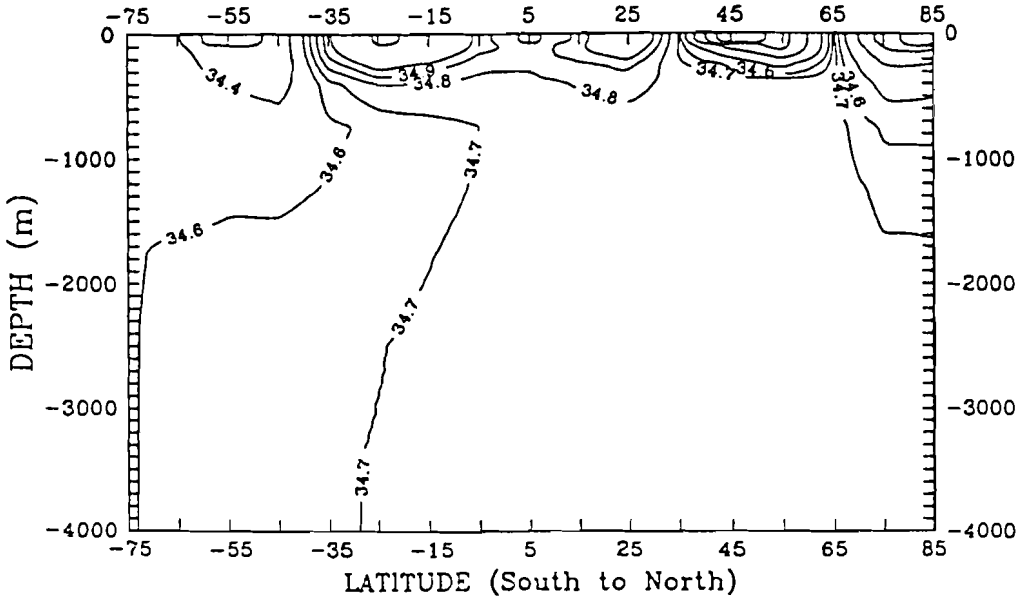

Fig. 4. Zonally averaged salinity field (ppt).

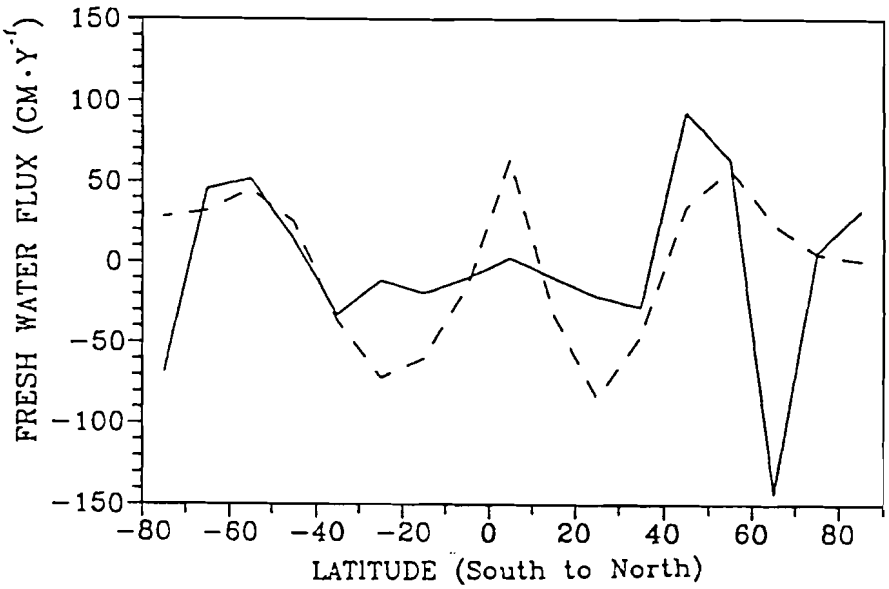

Fig. 5. The model values of surface fresh water flux (solid curve) together with the observation estimates of Baumgartner and Reichel (1975), (dashed curve).

agreement with observations presented by Baumgartner and Reichel (1975). Subtropical minima and the equatorial maximum are very weak in the model, while a very high negative freshwater flux is necessary to support the formation of deep water at high northern latitudes. The most evident explanation for this shortcoming is the combination of different ocean basins with their different freshwater budgets and circulations into one ocean basin.

The new parameterization of the baroclinic component of the vertical overturning allows to restrict the number of tuning parameters to only one in the description of ocean circulation (ε in Eq.20). The VOSF for present climate conditions is shown in Figure 6a. This field is similar to that presented in *WP1*, but with a more realistic maximum value in the Northern hemisphere (24Sv). The great similarity of the circulation pattern to that of the previous model version explains the close agreement between the meridional heat transport of both model versions (not shown here).

Finally, the distribution of the vertical diffusion coefficient A_z which is a function of the Brunt-Väisälä frequency in the present model version[1], is shown in Figure 7. A_z increases significantly from the surface layer to the bottom by one order of magnitude and more. The presence of a local minimum in the subtropical thermocline ($\sim$500 m depth) reflects the increase of vertical stability. The regions of deep water formation are characterized by maximum values of the vertical diffusion coefficient.

[1] In the version described in *WP1* the constant value of $A_z = 10^{-4}$ m^2/s was used.

a)

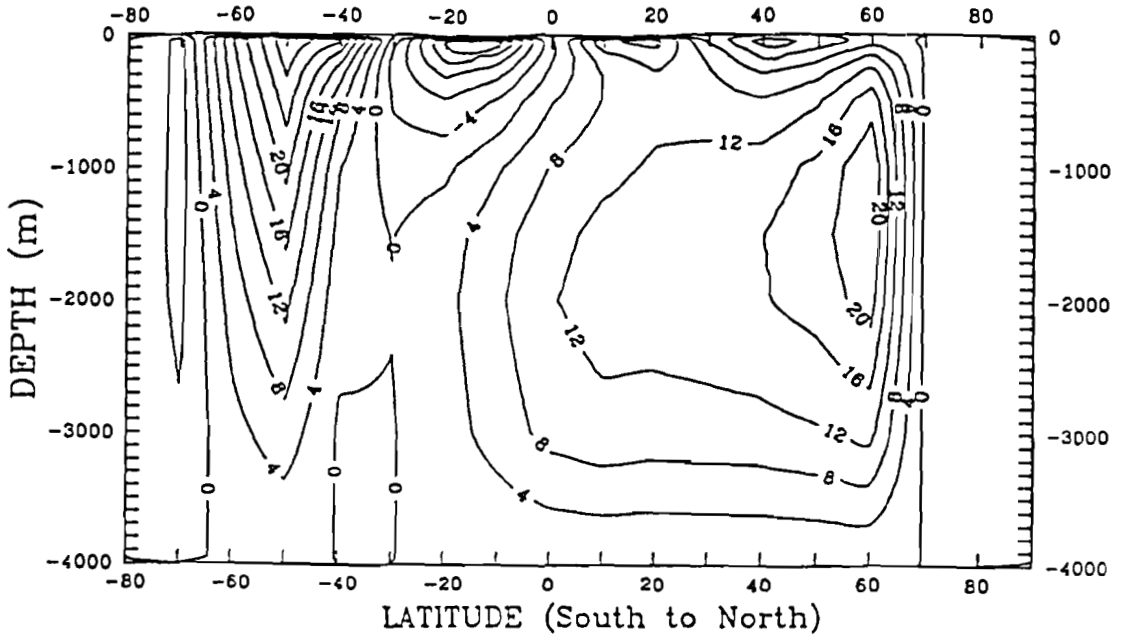

b)

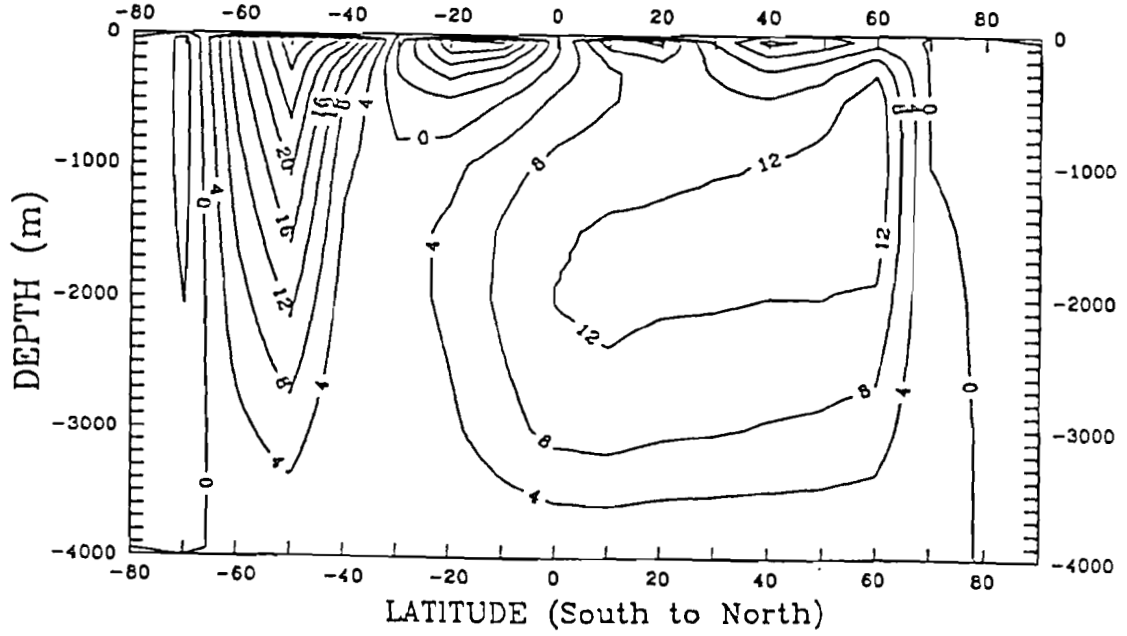

Fig. 6. The meridional streamfunction corresponding to the present climate (a), and at the end of the E Scenario (b).

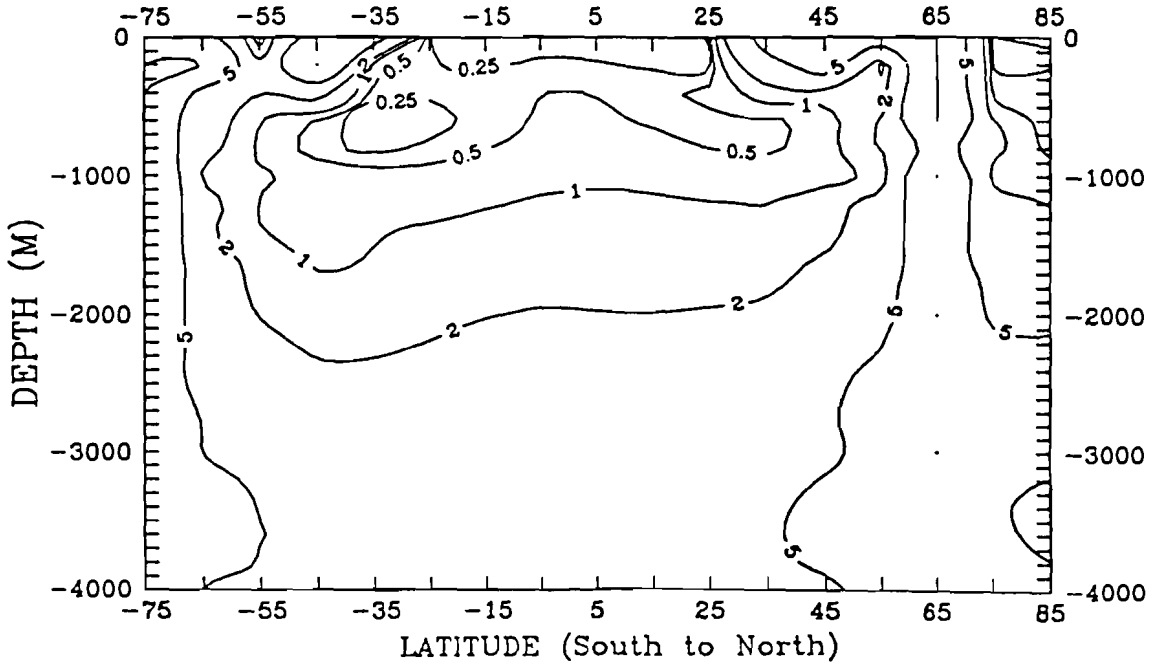

Fig. 7. The vertical diffusion coefficient (cm^2/s).

3.2 Internal variability

In contrast to the results described in *WP1*, an internal variability on the decadal time scale is present in the new results. Interesting as well is that the internal variability is very sensitive to freshwater flux. In two experiments with only a minor difference in the freshwater flux (less than 10%) different types of oscillations were observed. In the first experiment (Experiment I) oscillations in surface air temperature with a 30-year period are present in the subpolar region of the Southern hemisphere. In the second experiment (Experiment II) 7-year oscillations with a smaller amplitude appear in the subpolar region of the Northern hemisphere. Figure 8 shows these oscillations globally averaged, i.e., for globally averaged surface air temperature versus time. An analysis of the model results shows that thermohaline circulation and vertical convective mixing in the upper ocean layers are responsible for these oscillations.

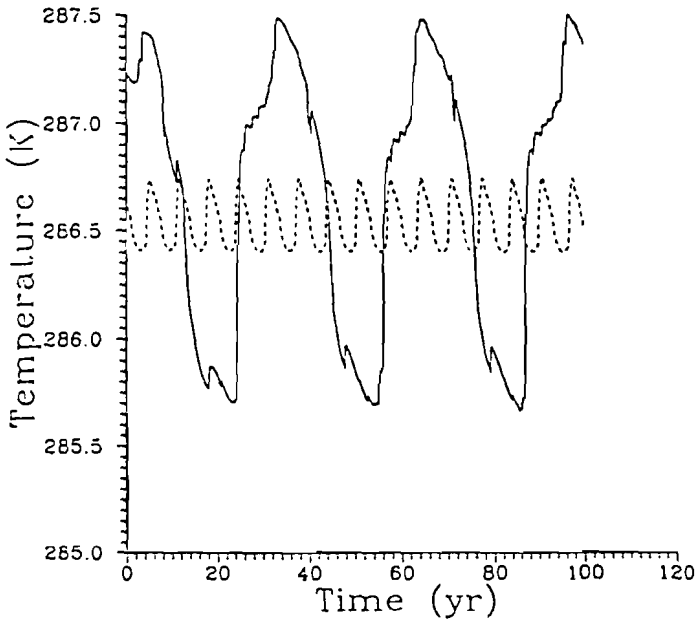

Fig. 8. Temporal variation of global surface air temperature for two different regimes of the internal variability. Solid line: Experiment I, dashed line: Exp. II (see text).

Figure 9 shows the simultaneous behaviour of the mixed layer temperature and vertical profile of salinity for that latitudinal belt, where the 30-year oscillations (Experiment I) were most pronounced. Abrupt increases of mixed layer temperature coincide with deep convection, penetrating down to 200 m depth. Warmer subsurface water mixes with colder and fresher surface water. The cooling of surface water is associated with a decrease in surface salinity, during which convective mixing ceases and the upper layer is isolated from subsurface layers. During this time, subsurface temperatures increase because of polarward advection of heat. These oscillations penetrate not deeper than 300 m and, as a result, they have only a small impact on the baroclinic circulation. It is of interest that oscillations with a similar period were observed in experiments with an oceanic GCM described by Weaver and Sarachnik (1991b). However, in their case, a much more significant perturbation of the baroclinic circulation and meridional heat transport took place. An internal variability ranging from a decadal to a century time scale was also observed in experiments with a similar but two-basin zonal ocean model (Stocker and Mysak, 1992).

In our model sea ice characteristics are parameterized in our model in terms of mixed laeyr temperature; therefore, sea ice fraction and thickness are also subjected to these oscillations. To elucidate the role of sea ice, we repeated Experiment I but with prescribed, time-independent sea ice fractions corresponding to the current mean annual estimates (Experiment I, modified), Figure 10. As follows from the figure, the period of the oscillations is the same, while the amplitude decreases approximately by a factor of two. One can conclude, therefore, that sea ice provides an important positive feedback for the internal variability of the model, but it is not the dominating mechanism.

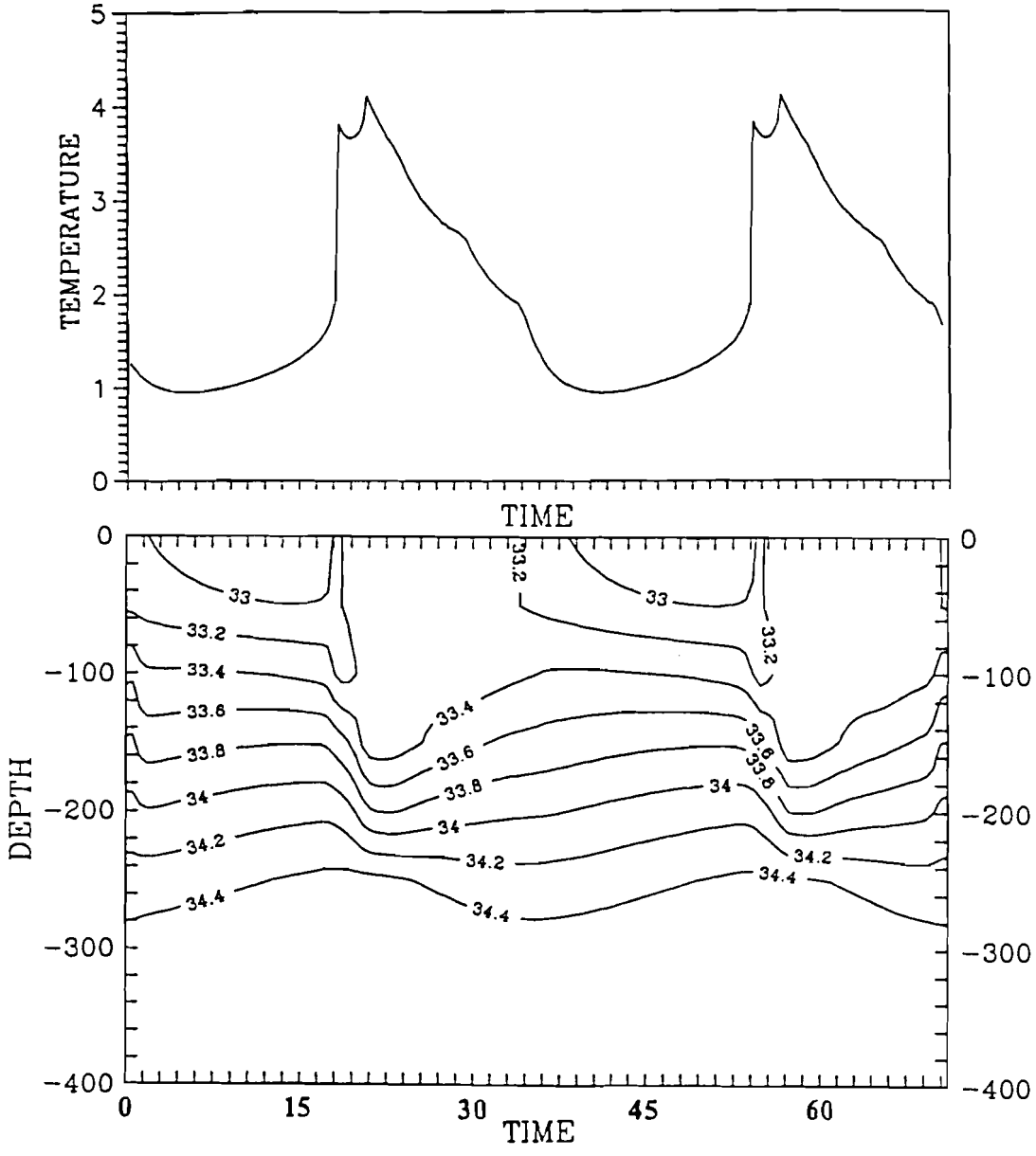

Fig. 9. Time evolution of surface temperature (°C) at the top and vertical profile of salinity (ppt) at the bottom in the latitudinal belt 50-60 S.

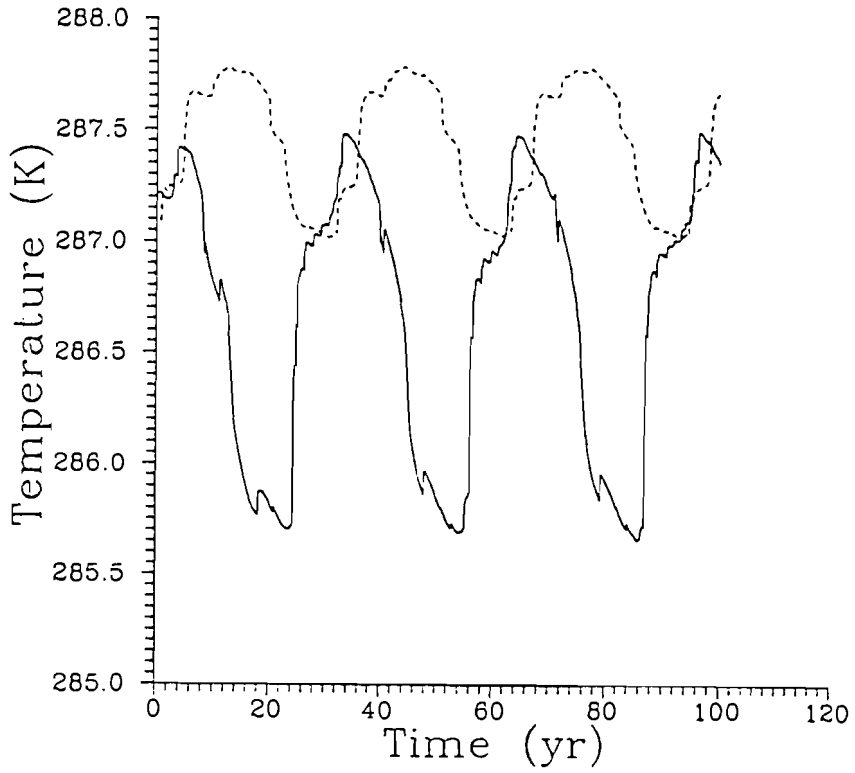

Fig. 10. The role of sea ice in regard to the internal variability of the model. Solid line: Experiment I; dashed line: Experiment I, modified (run with prescribed sea ice fractions, see text).

3.3 Climate sensitivity

The equilibrium response of the globally averaged surface air temperature to a doubling of CO_2 in the atmosphere (climate sensitivity) is one of the important characteristics of any climate model. According to the IPCC Reports (1990, 1992), the climate sensitivity is believed to lie within the interval $<1.5, 4.5\ K>$ with a best estimate of 2.5 K. Recent GCM experiments showed that a big part of the uncertainty is connected with the cloud feedback. Several simplified, nevertheless useful and widely used climate models, e.g., Wigley and Raper's (1990) model, are constructed in such a way that the climate sensitivity is the main external steering parameter. Its value dominates the behaviour of the climate model and, if the model is part of an integrated model (e.g., IMAGE 1.0, which was developed at RIVM in the Netherlands; Rotmans, 1990), the climate sensitivity has a profound bearing on the degree of various climatic impacts. An investigation of the uncertainty associated with the climate sensitivity is therefore one of the most important tasks.

The atmospheric part of the 2-D ZCM is part of IMAGE 2.0, the succeeding version of the Dutch integrated model (Alcamo et al., 1993). In this case, the climate sensitivity is not an external parameter any more, which can be chosen arbitrarily. Instead, the climate sensitivity is one of the inherent charasteristics of the climate model used. Therefore, it is highly desirable to study the uncertainty of the climate sensitivity of the model and to give priority to it when investigating the uncertainties of the entire integrated model.

The climate sensitivity of the previous model version described in *WP1* was 1.84 K, close to the lower limit of the IPCC interval. In this study, several changes in the atmospheric

component were made, as described above. The most important ones are 1. the use of a variable horizontal diffusion coefficient; 2. the inclusion of a lapse rate feedback (critical lapse rate for the convective adjustment dependent on surface air temperature); and 3. the replacement of the specific heat of dry air by the specific heat of moist air, which leads to modified conservation requirements. These changes result in a climate sensitivity of about 2.8 K, nearly 1 K higher in comparison with *WP1*.

To investigate this feature in more detail, the $2xCO_2$ equilibrium response of the surface air temperature above land is shown by latitude in Figure 11. The current result is compared with the result of the GFDL GCM (Manabe et al., 1990) and the previously published results of the 2-D model (*WP1*). Due to the higher climate sensitivity of the GFDL GCM (about 4 K), its surface air temperature values are higher; the latitudinal distribution of the response, however, is similar. Comparing the current results of the 2-D ZCM with those of *WP1*, we see that the increase in the climate sensitivity by one degree is caused first of all by the more pronounced temperature response of the model in mid latitudes. The same conclusion can be drawn from the latitudinal response of the oceanic mixed layer temperature (not shown).

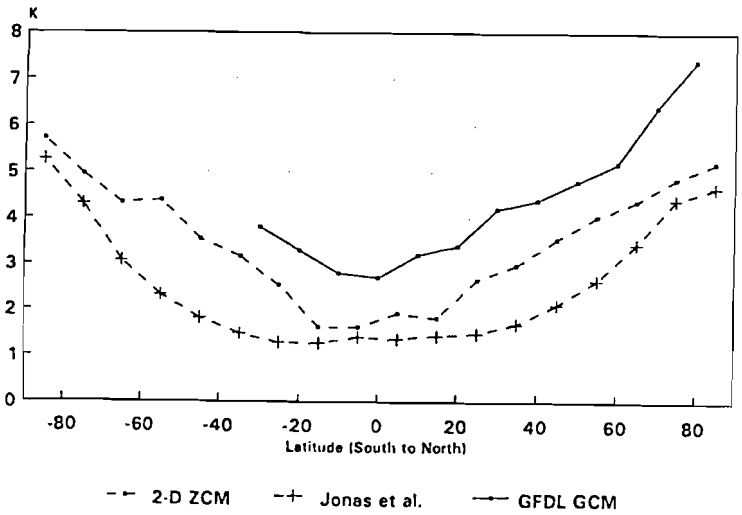

Fig. 11. Equilibrium response of surface air temperature above land to doubling of CO_2.

3.4 Time-dependent response

Scenario E of the IPCC 1992, which projects the highest increase in radiative forcing among the updated IPCC scenarios (IPCC, 1992), was used to force the model in a time-dependent mode. The time dependent concentrations of the following greenhouse gases were used: CO_2, CH_4, N_2O, CFC-11 and CFC-12. The spatial distribution of O_3 was kept constant in the run corresponding to the conditions in 1990. The run finishes in 2100.

The time-dependent experiment starts from the quasi-stationary stage reached at the end of Experiment II (small oscillations in the Northern hemisphere) with greenhouse gas concentrations corresponding to the year 1990 (t=0 in Figure 12). As an immediate reaction of the climate system, intensive oscillations in the Southern hemisphere similar to those observed in Experiment I appear. As a result, the globally averaged temperature drops by half a degree after 15 years of integration (t=15). Then similar temperature drops repeat with approximately the same period as in Experiment I. At the same time, small oscillations in the Northern hemisphere completely disappeared during the first 50 years of the run (t=50). Therefore, a progressive warming of the climate system caused by inreasing greenhouse gas concentrations results in a change of the internal variability. The global warming during a 100-year integration reaches approximately 3 °C, which seems to be in good agreement with GCM results of Cubasch et al. (1992), if we take into account slight differences in the scenarios used and in the climate sensitivities.

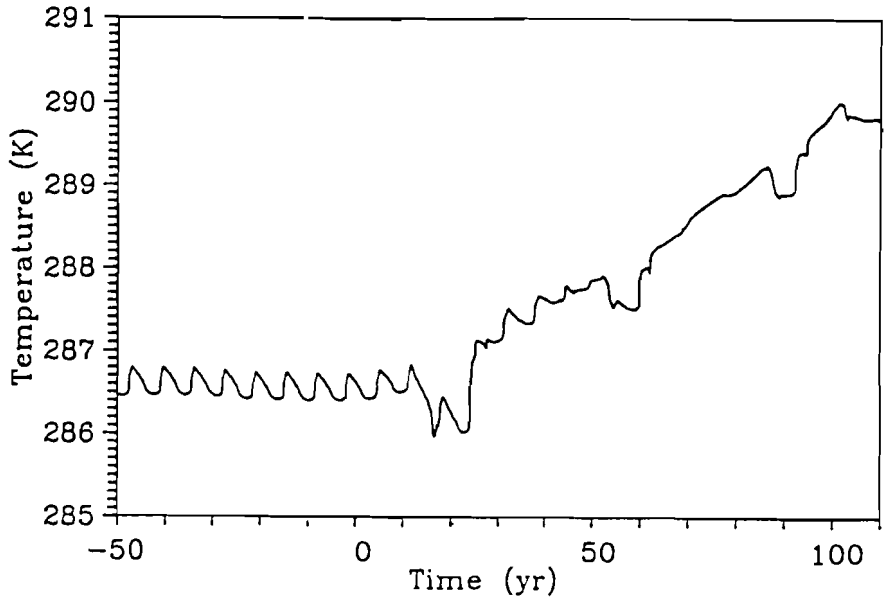

Fig. 12. Time evolution of the globally averaged surface ait temperature. Left part of the graph ($t<0$) represents behaviour of the climate system under present greenhouse gases concentration. At $t=0$ greenhouse gas concentrations begin to change according to the IPCC 1992 Scenario E.

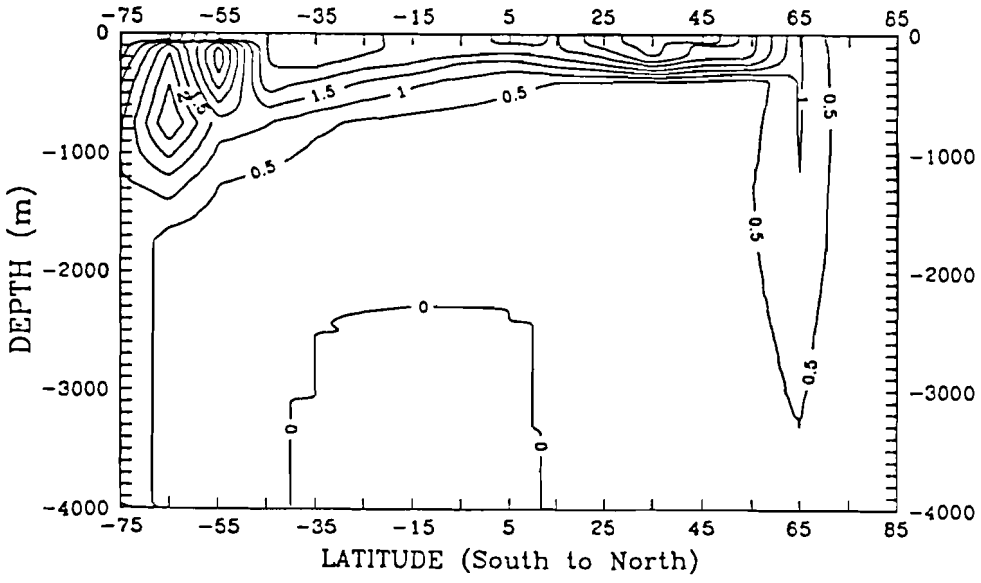

Fig. 13. Temperature anomalies in the ocean at the end of Scenario E (2100).

Temperature anomnalies in the ocean at the end of the experiment in 2100 are shown in Figure 13. The pattern in the Northern hemisphere is similar to that presented in *WP1* except for the smaller penetration depths of temperature anomalies caused by the weaker overturning and smaller vertical diffusion coefficient in the present model. The maximum warming of the ocean surface lies in the subtropics and reaches 3.5° C. A somewhat more complex pattern of temperature anomalies results in the Southern hemisphere. The surface temperature near the Antarctics decreases, but in subsurface layers the temperature increases due to a decrease in the convective mixing rate.

An important feature of global climate change that was recently revealed in coupled GCM experiments is a significant decay of vertical overturning caused by global warming (Cubash et al., 1992; Manabe and Stouffer, 1993). According to the results of Manabe and Stouffer (1993), the intensity of vertical overturning in the Northern hemisphere can decrease by a factor of two and more during 140 years of 1% increase of carbon dioxide concentration per year. The main reasons for this decay of vertical overturning are the increasing temperature and decreasing salinity in high latitudes, that both lead to a decrease of equator-pole density gradients in the ocean and, as a result, to a decay of baroclinic circulation. This change of the ocean circulation can possibly have an important impact on climate as well as on global geochemical cycles (Mikolajevicz et al., 1993). In our model results for scenario A, described in *WP1*, the vertical overturning also decreased but not as significantly (less than 10%). Results of the current model version (shown in Figures 6b and 14) seem to be more in agreement with the GCM results mentioned above. The most significant changes in the VOSF take place in the Northern hemisphere, where the vertical overturning has dropped by 40% by the end of the time-dependent run.

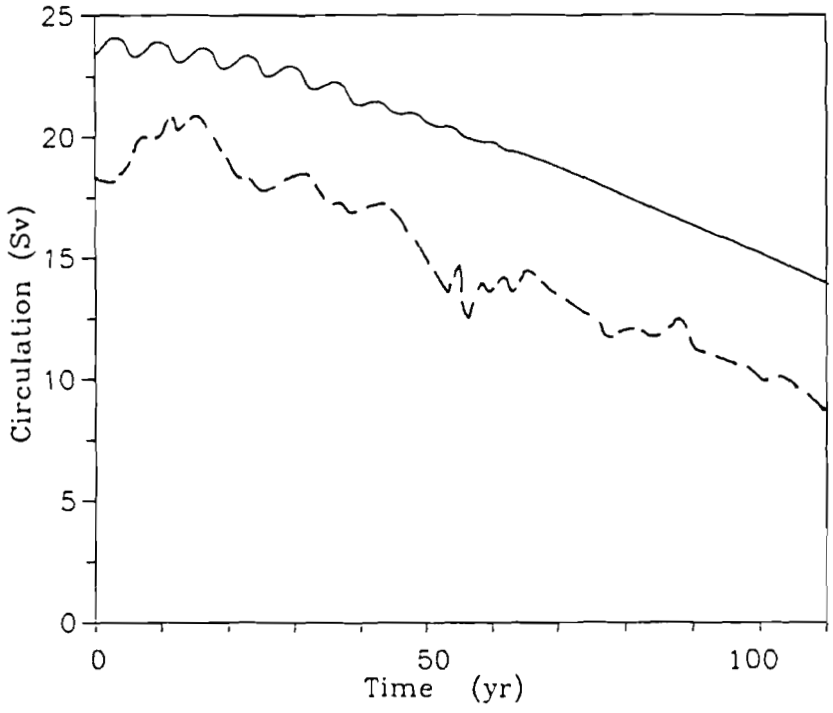

Fig. 14. Maximum of the vertical overturning in the Northern hemisphere for the IPCC 1992 Scenario E (solid line) compared with the results of Manabe and Stouffer (1993) for a 1% increase of CO_2 per year (their experiment 4xC, dashed line).

4. Conclusions

An improved version of the 2-D ZCM in comparison with that published in the preceding paper (*WP1*) was presented. The improvements were made in both the atmospheric part and the oceanic part of the model.

The modifications in the atmosphere lead to a closer agreement of the global energy distribution with current estimates and also to changes in the latitudinal distribution of some parameters such as albedo at the TOA and meridional heat transport. However, the main consequence is the increased climate sensitivity of the model - the current value is about 2.8 K. Investigation of various mechanisms which influence the climate sensitivity is useful especially if a climate model is part of an integrated model, because the climate sensitivity directly influences the degree of individual climate impacts.

The modifications in the ocean, first of all the inclusion of salinity as a prognostic variable, lead to a more complex behaviour of the whole coupled model, namely to the occurence of internal oscillations in the climate system on a decadal time scale. Two different modes of these oscillations are discussed in this paper: a) approximately 30-year oscillations in the Southern ocean, and b) 7-year oscillations in the northern subpolar region with an amplitude approximately half as great. The occurence of these modes is strongly dependent on the salinity flux at the ocean surface.

In case of the time dependent run according to the IPCC 1992 Scenario E, the internal temperature variability completely changed during the first 50 years of the model run. In

addition, the intensity of the vertical overturning in the Northern hemisphere significantly declined to the end of the experiment. This change in the oceanic circulation is not only in qualitative agreement, as it is the case in the experiments described in *WP1*, but also in quantitative agreement with state of the art coupled GCMs.

In our opinion, these results give additional support to the idea that simplified climate models can successfully reproduce important features of the climate system, consistent with much more sophisticated and computationally extremely expensive coupled GCMs. Such simplified climate models can then be used as a climate module of an appropriate (in the sence of spatial and temporal resolution) integrated model of climate change for solving broad range of scientific and applied tasks.

REFERENCES

Alcamo, J., G.J.J. Kreileman, M. Krol and G. Zuidema, (1993). Modelling the global society-biosphere-climate system. Part 1: Model description and testing. Submitted to *Water, Air and Soil Pollution.*

Baumgartner, A., and E. Reichel, (1975). *The world water balance: Mean annual global continental and maritime precipitation, evaporation and runoff.* R. Lee, translation, Elsevier, 179 pp.

Carissimo, B.C., A.H. Oort and T.H. Vonder Haar, (1985). Estimating the Meridional Energy Transports in the Atmosphere and the Ocean. *J. Phys. Oceanogr.* **15**, 82-91.

Cubasch, U., K. Hasselmann, H. Höck, E. Maier-Reimer, U. Mikolajewicz, B.D. Santer and R. Sausen, (1992). Time-Dependent Greenhouse Warming Computations with a Coupled Ocean-Atmosphere Model. *Climate Dynamics*, **8**, 55-69.

Cummins, F.P., G. Holloway, A.E.Garget, (1990). Sensitivity of the GFDL ocean general circulation model to a parameterization of vertical diffusion. *J. Phys. Oceanogr.*, **20**, 817-830.

Ellis, J.S. and T.H. Vonder Haar, (1976). Zonal Average Earth Radiation Budget Measurements from Satellites for Climate Studies. *Atmos. Sci. Paper 240*, Colorado State University, Fort Collins, Colorado, U.S.A.

Han, Y.-J. and S.-W.Lee, (1983). An analysis of monthly mean wind stress over the global ocean. *Mon. Wea. Rev.*, **111**, 1554-1566.

Intergovernmental Panel on Climate Change, (1990). *Climate Change 1990: The IPCC Scientific Assessment.* Working Group I, Cambridge University Press, Cambridge, U.K.

Intergovernmental Panel on Climate Change, (1992). *Climate Change 1992: The supplementary report to the IPCC Scientific Assessment.* Working Group I, Cambridge University Press, Cambridge, U.K.

Jonas, M., A.V. Ganopolski, J. Krabec, K. Olendrzynski and V.K. Petoukhov, (1993). A Set of Climate Models for Integrated Modelling of Climate Change Impacts. Part I: Introduction and Overview, A 2-D Zonal Climate Model, A Projected Application to European Forests. WP-93-58, IIASA, Austria (referred to as *WP1*).

Levitus, S., (1982). Climatological Atlas of the World Ocean. NOAA Prof. Pap. No. 13, US Government Printing Office, Washington, D.C.

Manabe, S. and R.J. Stouffer, (1988). Two stable equilibria of a coupled ocean-atmosphere model. *J. Climate*, **1**, 841-866.

Manabe, S., K. Bryan and M.J. Spelman, (1990). Transient Response of a Global Ocean-Atmosphere Model to a Doubling of Atmospheric Carbon Dioxide. *J. Phys. Oceanogr.*, **20**, 722-749.

Manabe, S. and R.J. Stouffer, (1993). Century-scale effects of increased atmospheric CO_2 on the ocean-atmosphere system. *Nature*, **364**, 215-218.

MacKay, R.M. and M.A.K. Khalil, (1991). Theory and Development of a One Dimensional Time Dependent Radiative Convective Climate Model. *Chemosphere*, **22**, 383-417.

Mikolajewicz, U., E. Maier-Reimer and A. Winguth, (1993). The effect of time-dependent ocean circulation on oceanic uptake of CO_2. *Research activities in atmospheric and oceanic modelling*, No. 18, ed. G.J.Boer, WMO, Switzerland.

Mochov, I.I., (1983). Tropospheric Lapse Rate and Its Empirical Relationship to Surface Air Temperature. Izvestia Acad. Sciences USSR, *FAO*, **19**, 913-919 (in Russian).

Peng, L., M.-D. Chou and A. Arking, (1987). Climate Warming due to Increasing Atmospheric CO_2: Simulations with a Multilayer Coupled Atmosphere-Ocean Seasonal Energy Balance Model. *J. Geophys. Res.* **92**(D5), 5505-5521.

Rotmans, J., (1990). *IMAGE: An Integrated Model to Assess the Greenhouse Effect.* Kluwer Academic Publishers, Dordrecht, The Netherlands.

Schneider, S.H., (1989). *Global Warming: Are We Entering the Greenhouse Century?* Sierra Club Books, San Francisco, 317 pp.

Sellers, W.D., (1973). A New Global Climatic Model. *J. Appl. Meteor.*, **12**, 241-254.

Smith, E.A. and M.R. Smith, (1987). Interannual Variability of the Tropical Radiation Balance and the Role of Extended Cloud Systems. *J. Atmos. Sci.*, **44**, 3210-3224.

Stocker, T.F. and L.A.Mysak, (1992). Climatic fluctuations on the century time scale: A review of high-resolution proxy data and possible mechanisms. *Climate Change*, **20**, 227-250.

UNESCO, (1981). The Practical Salinity scale 1978 and the International Equation of State of Seawater 1980. *Unesco Techn. Pap. in Mar. Sci.*, No. 36, 13-21.

Weaver, A.J. and E.S. Sarachnik, (1991a). The role of mixed boundary conditions in numerical models of the ocean's climate. *J. Phys. Oceanogr.*, **21**, 1470-1493.

Weaver, A.J. and E.S. Sarachnik, (1991b). Evidence for Decadal Variability in an Ocean General Circulation Model: An Advective Mechanism. *Atmosphere-ocean*, **29**, 197-231.

Wigley, T.M.L. and S.C.B. Raper, (1990). Natural Variability of the climate system and detection of the greenhouse effect. *Nature*, **344**, 324-327

Wright, D.G. and T.F. Stocker, (1991). A zonally averaged ocean model for the thermohaline circulation. Part I: Model development and flow dynamics. *J. Phys. Oceanogr.*, **21**, 1713-1724.